

Onset of collective excitations in the transverse dynamics of simple fluids

Eleonora Guarini ^{1,*}, Martin Neumann ², Alessio De Francesco ³, Ferdinando Formisano ³, Alessandro Cunsolo ⁴,
Wouter Montfrooij ⁵, Daniele Colognesi ⁶ and Ubaldo Bafle ⁶

¹*Dipartimento di Fisica e Astronomia, Università degli Studi di Firenze, via G. Sansone 1, I-50019 Sesto Fiorentino, Italy*

²*Fakultät für Physik der Universität Wien, Kolingasse 14-16, A-1090 Wien, Austria*

³*CNR-IOM & INSIDE@ILL c/o Operative Group in Grenoble (OGG) F-38042 Grenoble, France and Institut Laue Langevin (ILL), F-38042 Grenoble, France*

⁴*Department of Physics, University of Wisconsin at Madison, 1150 University Avenue, Madison, Wisconsin 53706, United States*

⁵*Department of Physics and Astronomy, University of Missouri, Columbia, Missouri 65211, United States*

⁶*Consiglio Nazionale delle Ricerche, Istituto di Fisica Applicata “Nello Carrara”, via Madonna del Piano 10, I-50019 Sesto Fiorentino, Italy*



(Received 9 June 2022; revised 29 October 2022; accepted 10 January 2023; published 30 January 2023)

A thorough analysis of the transverse current autocorrelation function obtained by molecular dynamics simulations of a dense Lennard-Jones fluid reveals that even such a simple system is characterized by a varied dynamical behavior with changing length scale. By using the exponential expansion theory, we provide a full account of the time correlation at wavevectors Q between the upper boundary of the hydrodynamic region and $Q_p/2$, with Q_p being the position of the main peak of the static structure factor. In the Q range studied, we identify and accurately locate the wavevector at which shear wave propagation starts to take place, and show clearly how this phenomenon may be represented by a damped harmonic oscillator changing, in a continuous way, from an overdamped to an underdamped condition. The decomposition into exponential modes allows one to convincingly establish not only the crossover related to the onset of transverse waves but, surprisingly, also the existence of a second pair of modes equivalent to another oscillator that undergoes, at higher Q values, a similarly smooth over to underdamped transition.

DOI: [10.1103/PhysRevE.107.014139](https://doi.org/10.1103/PhysRevE.107.014139)

I. INTRODUCTION

In the field of the microscopic dynamics of fluids, increasing attention has been paid in the last two decades to the study of shear waves. The propagation of both longitudinal and transverse acoustic waves depends not only on the thermodynamic state of the fluid but also on the length scale (i.e., on the inverse of the wavevector modulus $Q = |\mathbf{Q}|$) at which these processes are probed. However, contrary to what happens for ordinary sound, where propagating longitudinal waves also exist in the $Q \rightarrow 0$ limit, even in very dilute gases, these dependencies have a peculiar character in the transverse case because the propagation of shear waves in fluids takes place only when both the density and Q exceed certain threshold values [1].

The existence of such a transition between the absence and presence of propagating transverse excitations has attracted much interest due to its evident link with the viscoelastic nature of liquids [1–3], whereby the system responds in a solidlike way to a perturbation of sufficiently high frequencies and wavevectors, while slower and longer-wavelength perturbations dissipate through viscous relaxation processes.

The connection of the threshold Q value (often referred to in the literature as Q_{gap}) with the relaxation time that Maxwell first introduced to account for viscoelasticity has been even recently discussed [4].

One of the dynamical quantities that are also sensitive to transverse particle motions (i.e., orthogonal to \mathbf{Q}) is the velocity autocorrelation function [5,6]. Moreover, a widely debated issue concerns the visibility of transverse excitations in experimental determinations [7–11] and simulations [12–14] of the spectrum of density fluctuations, i.e., of the dynamic structure factor $S(Q, \omega)$, in liquid metals. However, the quantities that directly capture the essence of the transverse dynamics are the transverse current time autocorrelation function $C_T(Q, t)$ and its frequency spectrum $\tilde{C}_T(Q, \omega)$ [15]. Therefore, investigating the conditions that allow for the propagation of shear excitations requires the analysis of transverse current data at various Q values. However, before concentrating on specific features such as the excitation frequencies and damping rates and their Q dependence, and on the determination of Q_{gap} , a valid modeling of $C_T(Q, t)$ or $\tilde{C}_T(Q, \omega)$ should, in first place, provide an accurate representation of available data in the entire time or frequency ranges. Here data means simulation results, since $\tilde{C}_T(Q, \omega)$ is currently not accessible by spectroscopic techniques able to probe the picosecond and nanometer scales.

*Corresponding author: guarini@fi.infn.it

II. SIMULATION AND ANALYSIS

In this paper, we pursue this goal using molecular dynamics (MD) simulation data for a dense fluid of particles interacting with the Lennard-Jones 12–6 (LJ) potential

$$u(r) = 4\epsilon[(\sigma/r)^{12} - (\sigma/r)^6], \quad (1)$$

where ϵ and σ are the welldepth of the pair potential and the particle diameter, respectively. The thermodynamic state is defined by temperature $T = 1.35$ and number density $n = 0.8$. Here, T and n are dimensionless variables defined via the standard reduction through the LJ parameters ϵ and σ and the particle mass m . In terms of the corresponding absolute quantities, reduced temperature and density are given by $k_B T/\epsilon$ and $n\sigma^3$, respectively, while wavevector and angular frequency are expressed by $Q\sigma$ and $\omega\sqrt{m\sigma^2/\epsilon}$. Unless differently stated, throughout this paper we will always use reduced variables, but for ease of notation we will omit to mark them with the usual asterisk. In the (n, T) plane the chosen thermodynamic point is just above the critical temperature and at a density slightly lower than the triple point density.

The MD simulations were performed with the leapfrog algorithm in the isokinetic ensemble, using a cubic simulation volume, linked-list cells, a force cutoff $r_c = 6.5$, and a timestep $\delta t = 0.002$ [16]. The correlation functions were obtained as averages over ten independent subruns of 10^7 timesteps each, where averages over the subruns were used to estimate the error bars on the net correlation. The number of particles $N = 24805$ was chosen such that, with the required density, the minimum wavenumber compatible with the simulation cell has the value $Q_{\min} = 0.2$, and only wavevectors parallel to the three Cartesian axes were considered.

The computed $C_T(Q, t)$ was analyzed in the Q range between 0.2 and 3.4 in steps of 0.2. This range covers the first half of the region delimited by the position Q_p of the main peak of the static structure factor $S(Q)$, located in this system at $Q_p = 6.76$.

For the analysis of the MD data, we apply the exponential expansion theory (EET) [17–19], which allows for excellent descriptions of various correlation functions and spectra of interest for the self [5,6] and collective dynamics [11,20]. EET states that any autocorrelation function can be expressed as a series of exponential terms (called modes). Thus, for $t \geq 0$, we write, at each Q value

$$C_T(Q, t) = C_T(Q, 0) \sum_{j=1}^{\infty} I_j \exp(z_j t), \quad (2)$$

where both I_j and z_j can either be real or complex, with $\text{Re } z_j < 0$. A real mode describes the exponential decay of a relaxation process, while a pair of complex conjugate modes accounts for a propagating excitation with damping coefficient $-\text{Re } z_j$ and frequency $|\text{Im } z_j|$. In both cases, we shall refer to $-\text{Re } z_j$ as the “damping” of the mode. In Eq. (2), I_j and z_j are dependent on Q , although this will not be explicitly indicated in the following. We refer the reader to Refs. [5,6,11] for details on the application of EET, where a fitting procedure is applied to determine the parameters z_j and I_j of a small number p of modes to which the sum in Eq. (2) effectively reduces. Here we only note that $p - 1$

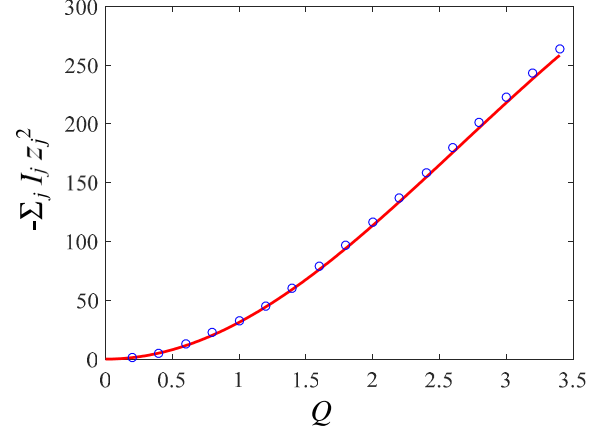


FIG. 1. Q dependence of the normalized second frequency moment as obtained from the fit parameters (blue circles) and from the theoretical prescription in Eq. (1.151) of Ref. [2] (red curve).

constraints have been imposed to the amplitudes I_j in order to enforce the correct short time behavior of the fitted $C_T(Q, t)$ [11]. The constraints are expressed as $\sum_{j=1}^p I_j = 1$, which follows directly from Eq. (2) at $t = 0$, and $\sum_{j=1}^p I_j z_j = 0$. In addition, as described below, $\sum_{j=1}^p I_j z_j^3 = 0$ was also applied beyond a certain Q value. However, we did not impose the constraint that $-\sum_{j=1}^p I_j z_j^2$ should equal the theoretically known second frequency moment of the normalized spectrum (see Eq. (1.151) of Ref. [2]). Therefore, the comparison of the second moment of the fitted spectrum with its theoretical value is a stringent test of the correctness of the fit results. Figure 1 shows that a very good agreement is found at all investigated Q values.

When performing fits in the time domain, it has to be remembered [16,21] that the use of periodic boundary conditions in MD may produce spurious effects in the calculated correlations beyond the so-called recurrence time $t_R = (N/n)^{1/3}/c_s$, i.e., the time required by a density wave to

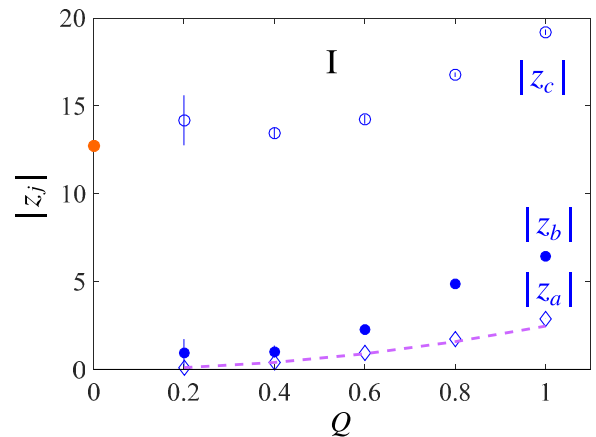


FIG. 2. Damping coefficients $|z_a|$, $|z_b|$, and $|z_c|$ of the three modes fitted to $C_T(Q, t)$ in range I. The dashed curve displays the $(\eta/n)Q^2$ hydrodynamic behavior. The orange dot at $Q = 0$ indicates the value of $1/\tau_M$.

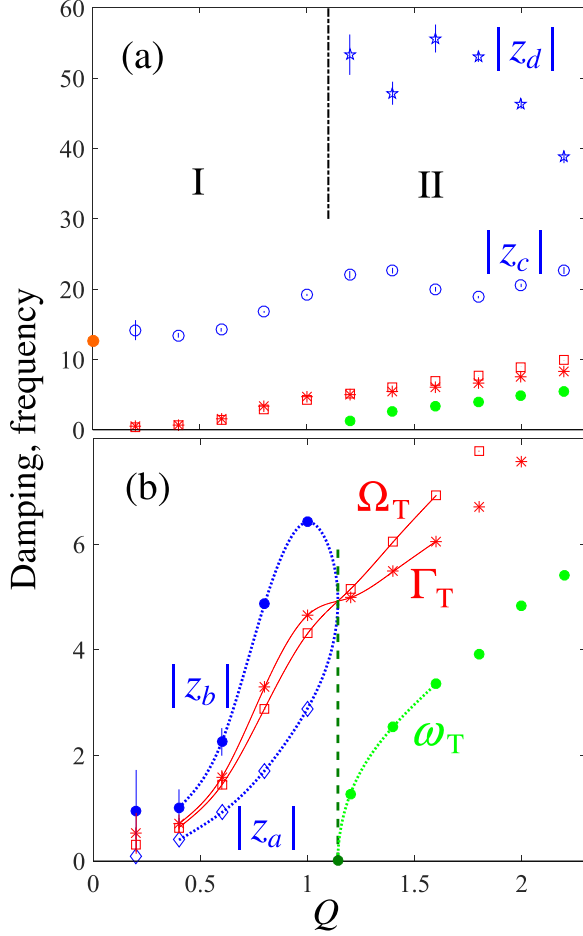


FIG. 3. Damping and frequency parameters from the fits to $C_T(Q, t)$ in ranges I and II. (a) The dampings of real modes c and d in range II are shown as blue circles and blue stars, respectively. Ω_T (red squares), Γ_T (red asterisks), and the propagation frequency ω_T (green dots) are shown. The orange dot at $Q = 0$ is the same as in Fig. 2. (b) Zoom of the low frequency region of frame (a), also showing $|z_a|$ and $|z_b|$ from Fig. 2. The red lines are spline interpolations of $\Omega_T(Q)$ and $\Gamma_T(Q)$ across the transition from the overdamped to the underdamped regime. The green dashed line marks the value of Q_{gap} . The dotted blue lines show the behavior of $|z_a|$ and $|z_b|$ in range I near the transition point. The dotted green line shows the beginning of the dispersion curve $\omega_T(Q)$.

propagate over the box length at the adiabatic sound speed c_s . In our case, with $c_s = 6.22$ [22], one has $t_R = 5$, which defines the maximum time value to be used for the fits. However, apart from the lowest Q 's, $C_T(Q, t)$ substantially decays to zero in a time shorter than t_R and the time range for the fit is accordingly further reduced to avoid inclusion of noisy and meaningless data displaying only statistical fluctuations around zero.

III. RESULTS

The hydrodynamic theory predicts that in the $Q \rightarrow 0$ limit $\tilde{C}_T(Q, \omega)$ has a Lorentzian shape with a half width at half maximum (HWHM) given by $(\eta/n)Q^2$ [23], where η is the

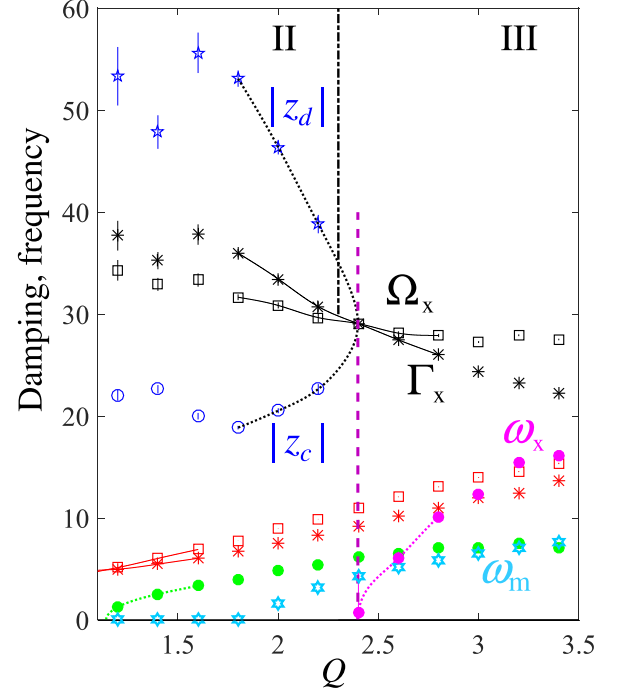


FIG. 4. Damping and frequency parameters from the fits to $C_T(Q, t)$ in ranges II and III. Besides the curves already displayed in Fig. 3, here we show Ω_x (black squares), Γ_x (black asterisks), and the propagation frequency ω_x of the second excitation (magenta full circles). The black lines are spline interpolations of $\Omega_x(Q)$ and $\Gamma_x(Q)$ across the transition from the overdamping to the underdamping regime of the second excitation. The purple dashed line marks the Q at which the transition takes place. The dotted black lines show the behavior of $|z_c|$ and $|z_d|$ in range II near the transition point. The dotted magenta line shows the initial part of the second dispersion curve. The cyan hexagons indicate the position $\omega_m(Q)$ of the maximum in each $\tilde{C}_T(Q, \omega)$ spectrum.

shear viscosity [2]. Such a Lorentzian spectrum obviously corresponds to retaining only one term in Eq. (2), when $C_T(Q, t)$ decays through a purely diffusive process. The hydrodynamic behavior should be obtained as the long wavelength limit of the more complex dynamics observed at higher Q .

The range of wavevectors included in this study is divided in three parts, labeled as I, II, and III in the following, where different sets of exponential modes are required to accurately fit the time dependence of $C_T(Q, t)$. Specifically, we find that in a rather narrow Q interval a variety of dynamical behaviors occurs, smoothly transitioning from one Q regime into the other. The best-fitting parameters z_j are reported as functions of Q in Figs. 2–4, and their respective amplitudes I_j are displayed in Fig. 5. The MD data for $C_T(Q, t)$, the fitted exponential-mode curve, and its various components are shown in Figs. 6–8, one for each of the three Q regions. Each figure also shows the corresponding spectrum and its components.

In range I ($0.2 \leq Q \leq 1.0$), very good fits to $C_T(Q, t)$ are obtained when three real exponential terms are included in Eq. (2). The three modes, identified by subscripts a , b , and c , decay to zero with respective damping constants $|z_a|$, $|z_b|$,

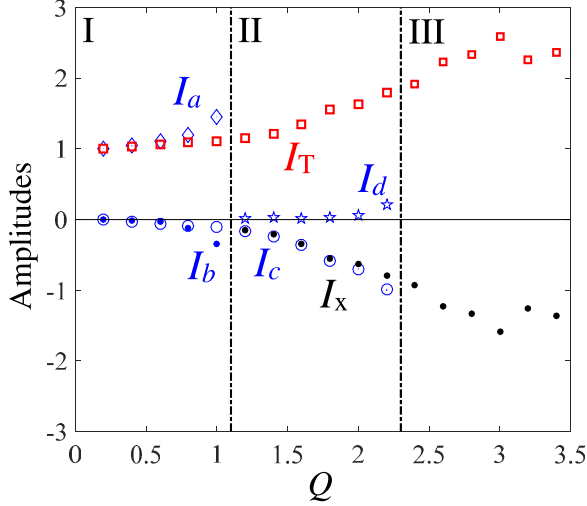


FIG. 5. Q dependence of the amplitudes of the fitted modes. Blue symbols refer to the real mode amplitudes: I_a (diamonds) and I_b (dots) in range I, I_c (circles) in ranges I and II, I_d (stars) in range II. The amplitudes I_T of the transverse oscillator and I_x of the second oscillator are also shown as red squares and black dots, respectively.

and $|z_c|$, shown in Fig. 2, which are the HWHMs of the three Lorentzian lines composing the spectrum. Mode a , with the smallest damping, is the dominant one ($I_a \geq 1$ in Fig. 5), while I_b and I_c are negative and vanish for $Q \rightarrow 0$ but increase slowly, in absolute value, with growing Q . We find that $|z_a|$ grows initially as Q^2 with a prefactor in full agreement with the quantity $(\eta/n)Q^2$ mentioned above (the LJ viscosity at our thermodynamic state is $\eta = 1.971$ [22]). We also remark that, while $|z_b|$ starts from zero, too, the width $|z_c|$ of the third Lorentzian line is only weakly dependent on Q and does not vanish for $Q \rightarrow 0$, where it approaches a value close to the reciprocal of the Maxwell time $\tau_M = \eta/G_\infty$, where G_∞ is the infinite-frequency shear modulus [24,25]. Overall, the low- Q dynamics complies with the hydrodynamic limit, but the detailed analysis in terms of three exponential modes elucidates a slight, yet clearly progressive, deviation from the limiting behavior.

In range II ($1.2 \leq Q \leq 2.2$), the above three-mode model becomes insufficient for an accurate description of the data, and four modes are now required, two of which are complex and two real. One of the latter is labeled c because both its damping $|z_c|$ and amplitude I_c evolve very smoothly from the corresponding parameters of the c mode of range I, indicating that the same relaxation process is present in both Q ranges [see Figs. 3(a) and 5]. The other, labeled as d , has a very large damping $|z_d|$ and despite its almost negligible amplitude, is necessary to reach a high fit quality. In fact, the last two panels of Fig. 7 show that a simpler fit model excluding the low-intensity mode d fails in accounting for the tails of the spectra and, at $Q = 1.4$ and 2.2 , gives a reduced χ^2 respectively 5 and 200 times larger than that of the four-mode fits.

The remaining two modes fitted to $C_T(Q, t)$ in range II form a pair of complex conjugate terms in Eq. (2). It is well known [26,27] that such a pair describes the dynamics of a

damped harmonic oscillator¹ characterized by an undamped frequency Ω_T , a damping Γ_T , and, when $\Omega_T > \Gamma_T$, an actual oscillation frequency $\omega_T = \sqrt{\Omega_T^2 - \Gamma_T^2}$. For the two modes, again denoted as a and b for the reasons explained below, one has $z_{a,b} = -\Gamma_T \pm i\omega_T$. Therefore, the two complex modes contribute to the total $C_T(Q, t)$ with an oscillatory underdamped component corresponding to a propagating collective excitation.

However, if the above condition were reversed, with $\Omega_T < \Gamma_T$, overdamping would occur and no oscillation would appear. The two modes would become real, with damping constants given by $z_{a,b} = -\Gamma_T \pm \sqrt{\Gamma_T^2 - \Omega_T^2}$. In both damping conditions it is seen that $\Omega_T^2 = z_a z_b$ and $\Gamma_T = -(z_a + z_b)/2$. It is then natural to check whether modes a and b determined in range I can be interpreted as representing an overdamped oscillator which evolves smoothly into the underdamped one defined in range II by Ω_T and Γ_T . Therefore, also in range I, we define $\Omega_T^2 = z_a z_b$ and $\Gamma_T = -(z_a + z_b)/2$ and observe that both $\Omega_T(Q)$ and $\Gamma_T(Q)$, reported in Fig. 3, have a smooth Q dependence in the whole range $0.2 \leq Q \leq 2.2$. Remarkably, the sum of the amplitudes of the two modes $I_T = I_a + I_b$ also displays a very smooth crossing of the boundary between range I and II (see Fig. 5).

We can thus confidently recognize modes a and b as present in both ranges I and II. Since mode a was seen to account for the transverse dynamics in the hydrodynamic limit, we conclude that the onset of the propagating transverse excitation is properly described as the transition of an oscillator from a low- Q overdamping condition ($\Omega_T < \Gamma_T$) to an oscillating one ($\Omega_T > \Gamma_T$). This justifies the use of a single suffix “T” to label the transverse modes. As shown in Fig. 3(b), the point where the spline interpolations of $\Omega_T(Q)$ and $\Gamma_T(Q)$ cross each other, which by definition is Q_{gap} , is determined with great accuracy to be $Q_{\text{gap}} = 1.14$, and the dispersion curve of the transverse excitation

$$\omega_T(Q) = \sqrt{\Omega_T^2(Q) - \Gamma_T^2(Q)} \quad (3)$$

is found, where we explicitly indicated the Q dependence of *both* quantities under the square root. From the interpolated values of Ω_T and Γ_T in range I the behavior of the real-mode damping coefficients $|z_a|$ and $|z_b|$ is obtained in the vicinity of the transition point, where they approach each other and eventually merge into Γ_T .

¹When such an oscillator is employed to model a collective excitation, it is usually referred to by its acronym DHO. However, when the global dynamics is described by more than two modes, the constraints to the mode amplitudes must be applied to the whole set of modes, and not simply to the two modes representing the oscillator. This fact modifies the expression of the amplitudes with respect to that of the “pure” DHO model [26,27]. Therefore, although the oscillators referred to here are indeed harmonic and damped, in order to prevent ambiguities and possible misunderstandings we avoid using the acronym DHO.

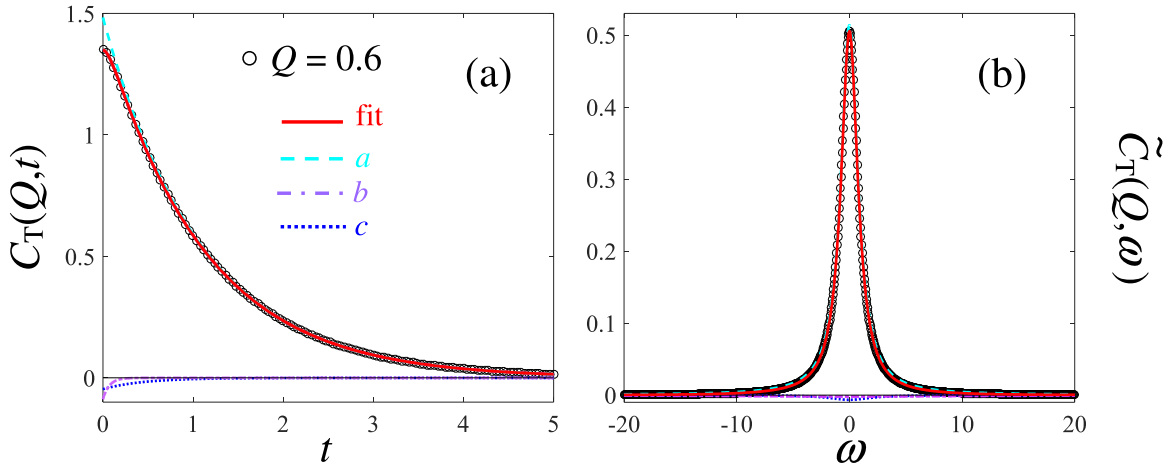


FIG. 6. (a) $C_T(Q, t)$ at a Q representative of region I (black circles). The fit result and its components are specified in the legend according to the labeling of the real modes described in the main text. (b) Corresponding spectrum and fit components.

Figure 7 displays the spectra at $Q = 1.4$ and 2.2 in order to show how a double peak develops in the spectrum only above a certain Q value, while at lower Q , despite the clear oscillatory component found by the fit procedure in range II, the spectrum does not (apparently) display any inelastic feature.

Finally, in range III ($2.4 \leq Q \leq 3.4$), best fits are also obtained with a four-exponential model for $C_T(Q, t)$, but now all modes are complex, two of which provide an impressively smooth continuation to larger Q of the propagating transverse excitation described by $\Omega_T(Q)$, $\Gamma_T(Q)$, and $I_T(Q)$ (see Figs. 4 and 5). The other complex pair of modes is seen to arise from the modes denoted as c and d in range II, with exactly the same kind of transition process from over to underdamping discussed before for the transverse excitation. Thus, the data display the onset of a second collective excitation characterized by the undamped frequency $\Omega_x(Q)$ and the damping $\Gamma_x(Q)$, which in range II are obtained as $\Omega_x^2 = z_c z_d$ and $\Gamma_x = -(z_c + z_d)/2$ and in range III are determined directly as fit parameters. Therefore, at the transition point, located at $Q = 2.4$ as the crossing point of spline interpolations of Ω_x and Γ_x , a second dispersion curve $\omega_x(Q) = \sqrt{\Omega_x^2(Q) - \Gamma_x^2(Q)}$ emerges, with a larger slope than that of ω_T .

The transverse dispersion curve $\omega_T(Q)$ cannot be determined unless it is obtained from the frequencies of the oscillatory components of $C_T(Q, t)$ at each Q value. This requires the exponential-mode description, either in the form used here or in the so-called generalized collective modes approach [28]; however, in the latter case, the modes are not fitted to the data. By contrast, the dispersion curve is usually obtained as the frequency position $\omega_m(Q)$ of the maxima of the individual $\tilde{C}_T(Q, \omega)$ spectra. The result of such a procedure is also shown in Fig. 4 (cyan hexagons). Since in the present case the spectra show a double-peaked top for $Q \geq 2.0$ only, this method gives for Q_{gap} a value between 1.8 and 2.0, quite larger than the already found $Q_{\text{gap}} = 1.14$. The values of $\omega_m(Q)$ not only fail to reproduce the correct frequencies ω_T , but also do not allow to detect the second excitation ω_x in range III. In fact, for $Q \geq 2.0$ the shape of $\tilde{C}_T(Q, \omega)$ does not show any visible difference in passing

from the one-excitation to the two-excitation dynamics (see Figs. 7 and 8).

As far as the second excitation is concerned, a double structure in $\tilde{C}_T(Q, \omega)$ has been found in *ab initio* simulations of some liquid metals [29], though in some cases only at very high pressures [30,31]. Interestingly, in Ref. [6] it has also been shown that the transverse current spectra of liquid gold display a clear shoulder at frequencies rather close to the maximum frequency of the sound dispersion curve. Moreover, a mixing of longitudinal and transverse excitations of $C_T(Q, \omega)$ was observed in water [32] and methanol [33]. Here, it is useful to note that, at our highest Q , the dispersion curve $\omega_x(Q)$ attains values that already exceed the transverse frequency ω_T by a factor ≈ 2 . Therefore, although we cannot make any ultimate statement or claim on the nature of the second excitation, we suggest that it may be related to the coupling between the longitudinal and transverse dynamics even in this much simpler fluid.

IV. CONCLUSIONS

We have shown that an EET analysis of $C_T(Q, t)$ allows for a very accurate representation of the simulated data at all the investigated wavevectors. The fitting of exponential modes reveals a rich dynamical behavior and enables a consistent interpretation through the simple concept of damped harmonic oscillators, discussed in detail in Refs. [26,27], whose intuitive meaning is that relaxation and propagation phenomena are driven by the competition between “elastic” forces and viscous dissipation, represented by the undamped frequencies (Ω_T or Ω_x) and the damping coefficients (Γ_T or Γ_x), respectively. In this way, detailed properties of the transverse collective dynamics are revealed, including the appearance of a second excitation so far undetected in simple nonmetallic fluids, besides the expected emergence of the transverse mode propagation. Moreover, a very accurate determination of the threshold Q values is made possible. This work shows that in the Q evolution of $C_T(Q, t)$, the whole intensity, initially associated with a single hydrodynamic decay channel, smoothly

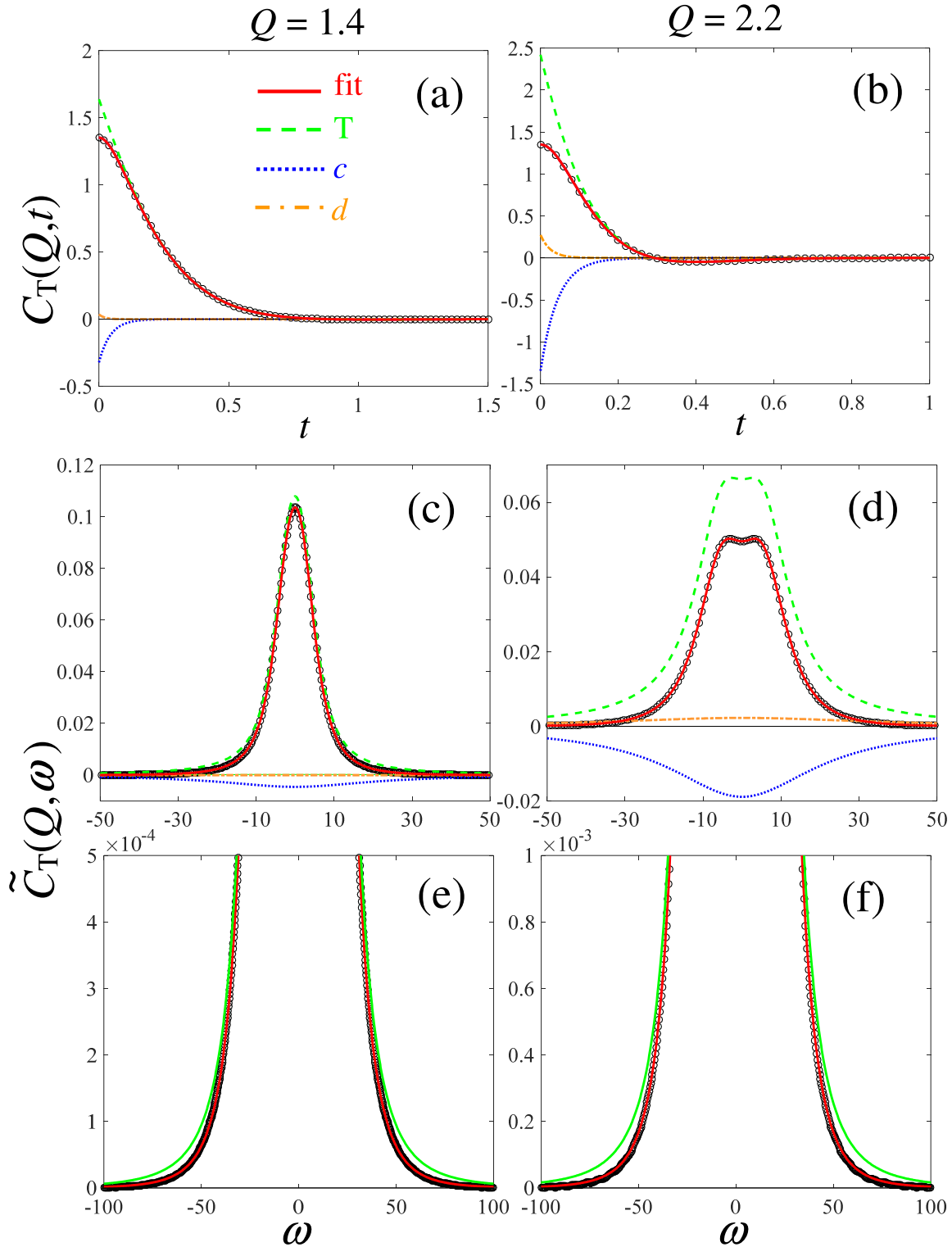


FIG. 7. (a)–(d) $C_T(Q, t)$ and its spectrum at two Q values in region II. Data are shown as black circles. The propagating transverse wave (T component) is shown as a dashed green curve. The real modes c and d are displayed as a dotted blue and a dot dashed orange curve, respectively. (e) and (f) Comparison of the fits shown in panels (c) and (d) (red curve) with fits performed by excluding mode d (green curve).

redistributes among four modes which give rise, in pairs, to the onset of two propagating excitations. An essential requirement for such an analysis is the accurate description of the entire time dependence of $C_T(Q, t)$ in terms of exponential

modes, where the choice of the number and nature of the modes to be fitted must be made at each Q by duly comparing the fit quality of different models, while avoiding unjustified overparametrizations.

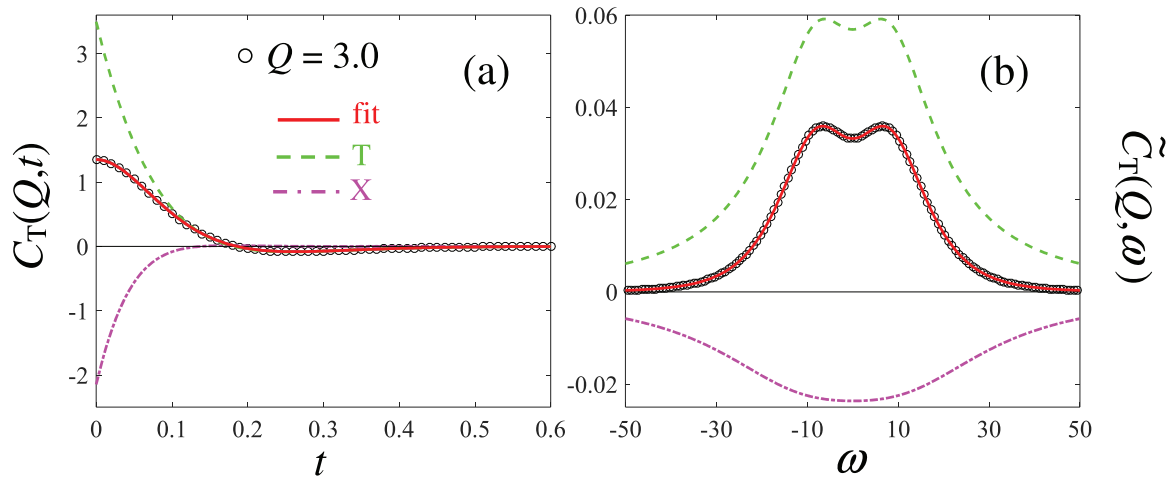


FIG. 8. Same as Fig. 6, but for region III. The propagating waves are shown as a dashed green and a dot dashed magenta curves for the T and X components, respectively.

ACKNOWLEDGMENTS

This research was funded by Ministero dell’Istruzione dell’Università e della Ricerca Italiano (Grant No. PRIN2017-

2017Z55KCW). We are greatly indebted to Walter Penits for technical support of the simulations.

- [1] D. Levesque, L. Verlet, and J. Kürkijarvi, Computer “experiments” on classical fluids. IV. Transport properties and time-correlation functions of the Lennard-Jones liquid near its triple point, *Phys. Rev. A* **7**, 1690 (1973).
- [2] U. Balucani and M. Zoppi, *Dynamics of the Liquid State* (Clarendon Press, Oxford, 1994).
- [3] A. Cunsolo, *The THz Dynamics of Liquids Probed by Inelastic x-Ray Scattering* (World Scientific, Singapore, 2021).
- [4] C. Yang, M. T. Dove, V. V. Brazhkin, and K. Trachenko, Emergence and Evolution of the k Gap in Spectra of Liquid and Supercritical States, *Phys. Rev. Lett.* **118**, 215502 (2017); See also the Comment to this Letter by T. Bryk, I. Mryglod, G. Ruocco, and T. Scopigno, *ibid.* **120**, 219601 (2018).
- [5] S. Bellissima, M. Neumann, E. Guarini, U. Bafile, and F. Barocchi, Density of states and dynamical crossover in a dense fluid revealed by exponential mode analysis of the velocity autocorrelation function, *Phys. Rev. E* **95**, 012108 (2017).
- [6] E. Guarini, S. Bellissima, U. Bafile, E. Farhi, A. De Francesco, F. Formisano, and F. Barocchi, Density of states from mode expansion of the self-dynamic structure factor of a liquid metal, *Phys. Rev. E* **95**, 012141 (2017).
- [7] S. Hosokawa *et al.*, Transverse Acoustic Excitations in Liquid Ga, *Phys. Rev. Lett.* **102**, 105502 (2009).
- [8] V. M. Giordano and G. Monaco, Fingerprints of order and disorder on the high-frequency dynamics of liquids, *Proc. Natl. Acad. Sci. USA* **107**, 21985 (2010).
- [9] S. Hosokawa *et al.*, Transverse excitations in liquid Sn, *J. Phys.: Condens. Matter* **25**, 112101 (2013).
- [10] M. Zanatta, F. Sacchetti, E. Guarini, A. Orecchini, A. Paciaroni, L. Sani, and C. Petrillo, Collective Ion Dynamics in Liquid Zinc: Evidence for Complex Dynamics in a Non-Free-Electron Liquid Metal, *Phys. Rev. Lett.* **114**, 187801 (2015).
- [11] E. Guarini, A. De Francesco, U. Bafile, A. Laloni, B. G. del Rio, D. J. González, L. E. González, F. Barocchi, and F. Formisano, Neutron Brillouin scattering and ab initio simulation study of the collective dynamics of liquid silver, *Phys. Rev. B* **102**, 054210 (2020).
- [12] M. Marqués, L. E. González, and D. J. González, *Ab initio* study of the structure and dynamics of bulk liquid Fe, *Phys. Rev. B* **92**, 134203 (2015).
- [13] B. G. del Rio, O. Rodriguez, L. E. González, and D. J. González, First principles determination of static, dynamic and electronic properties of liquid Ti near melting, *Comput. Mater. Sci.* **139**, 243 (2017).
- [14] B. G. del Rio, L. E. González, and D. J. González, *Ab initio* study of several static and dynamic properties of bulk liquid Ni near melting, *J. Chem. Phys.* **146**, 034501 (2017).
- [15] For the definition of $C_T(Q, t)$ we follow Ref. [2].
- [16] M. P. Allen and D. J. Tildesley, *Computer Simulation of Liquids* (Clarendon Press, Oxford, 1987).
- [17] F. Barocchi, U. Bafile, and M. Sampoli, Exact exponential function solution of the generalized Langevin equation for autocorrelation functions of many-body systems, *Phys. Rev. E* **85**, 022102 (2012).
- [18] F. Barocchi and U. Bafile, Expansion in Lorentzian functions of spectra of quantum autocorrelations, *Phys. Rev. E* **87**, 062133 (2013).
- [19] F. Barocchi, E. Guarini, and U. Bafile, Exponential series expansion for correlation functions of many-body systems, *Phys. Rev. E* **90**, 032106 (2014).
- [20] E. Guarini *et al.*, Collective dynamics of liquid deuterium: Neutron scattering and approximate quantum simulation methods, *Phys. Rev. B* **104**, 174204 (2021).
- [21] J. P. Hansen and I. R. McDonald, *Theory of Simple Liquids* (Academic Press, London, 1986).

- [22] K. Meier, Computer simulation and interpretation of the transport coefficients of the Lennard-Jones model fluid, PhD. thesis, University of the Federal Armed Forces Hamburg, 2002.
- [23] In absolute units, the halfwidth is given by $\eta/(nm)Q^2$ [2].
- [24] The infinite-frequency shear modulus can be computed from $G_\infty = nT + (2\pi/15)n^2 \int_0^\infty dr g(r)(df(r)/dr)$, with $f(r) = r^4 du(r)/dr$ where $u(r)$ is the interaction potential and $g(r)$ is the pair distribution function. The corresponding expression in absolute units is $G_\infty = nk_B T + (2\pi/15)n^2 \int_0^\infty dr g(r)(df(r)/dr)$ [25].
- [25] R. Zwanzig and R. D. Mountain, High-frequency elastic moduli of simple fluids, *J. Chem. Phys.* **43**, 4464 (1965).
- [26] U. Bafile, E. Guarini, and F. Barocchi, Collective acoustic modes as renormalized damped oscillators: Unified description of neutron and x-ray scattering data from classical fluids, *Phys. Rev. E* **73**, 061203 (2006).
- [27] W. Montfrooij, U. Bafile, and E. Guarini, Modeling of neutron and x-ray scattering by liquids: The risks of using phenomenological models, *Phys. Fluids* **33**, 087114 (2021).
- [28] I. M. Mryglod, Generalized statistical hydrodynamics of fluids: Approach of generalized collective modes, *Condens. Matter Phys.* **1**, 753 (1998).
- [29] B. G. del Rio and L. E. González, Longitudinal, transverse, and single-particle dynamics in liquid Zn: *Ab initio* study and theoretical analysis, *Phys. Rev. B* **95**, 224201 (2017).
- [30] T. Bryk, G. Ruocco, T. Scopigno, and A. P. Seitsonen, Pressure-induced emergence of unusually high-frequency transverse excitations in a liquid alkali metal: Evidence of two types of collective excitations contributing to the transverse dynamics at high pressures, *J. Chem. Phys.* **143**, 104502 (2015).
- [31] N. Jakse and T. Bryk, Pressure evolution of transverse collective excitations in liquid Al along the melting line, *J. Chem. Phys.* **151**, 034506 (2019).
- [32] M. Sampoli, G. Ruocco, and F. Sette, Mixing of Longitudinal and Transverse Dynamics in Liquid Water, *Phys. Rev. Lett.* **79**, 1678 (1997).
- [33] S. Bellissima, S. De Panfilis, U. Bafile, A. Cunsolo, M. A. González, E. Guarini, and F. Formisano, The hydrogen-bond collective dynamics in liquid methanol, *Sci. Rep.* **6**, 39533 (2016).